ELSEVIER

Marine Geology 225 (2006) 191–208

MARINE GEOLOGY
INTERNATIONAL JOURNAL OF MARINE GEOLOGY, GEOCHEMISTRY AND GEOPHYSICS

www.elsevier.com/locate/margeo

Pore water geochemistry of eastern Mediterranean mud volcanoes: Implications for fluid transport and fluid origin

Ralf R. Haese [a,*], Christian Hensen [b], Gert J. de Lange [a]

[a] *Department of Geochemistry, Faculty of Earth Sciences, Utrecht University, P.O. Box 80021, 3508 TA Utrecht, The Netherlands*
[b] *Leibniz-Institute of Marine Sciences (IFM-GEOMAR) and SFB 574, Marine Biogeochemistry, Wischhofstr. 1-3, D-24148 Kiel, Germany*

Received 6 August 2004; received in revised form 4 August 2005; accepted 2 September 2005

Abstract

The pore water chemistry of mud volcanoes from the Olimpi Mud Volcano Field and the Anaximander Mountains in the eastern Mediterranean Sea have been studied for three major purposes: (1) modes and velocities of fluid transport were derived to assess the role of (upward) advection, and bioirrigation for benthic fluxes. (2) Differences in the fluid chemistry at sites of Milano mud volcano (Olimpi area) were compiled in a map to illustrate the spatial heterogeneity reflecting differences in fluid origin and transport in discrete conduits in near proximity. (3) Formation water temperatures of seeping fluids were calculated from theoretical geothermometers to predict the depth of fluid origin and geochemical reactions in the deeper subsurface.

No indications for downward advection as required for convection cells have been found. Instead, measured pore water profiles have been simulated successfully by accounting for upward advection and bioirrigation. Advective flow velocities are found to be generally moderate (3–50 cm y^{-1}) compared to other cold seep areas. Depth-integrated rates of bioirrigation are 1–2 orders of magnitude higher than advective flow velocities documenting the importance of bioirrigation for flux considerations in surface sediments. Calculated formation water temperatures from the Anaximander Mountains are in the range of 80 to 145 °C suggesting a fluid origin from a depth zone associated with the seismic decollement. It is proposed that at that depth clay mineral dehydration leads to the formation and advection of fluids reduced in salinity relative to sea water. This explains the ubiquitous pore water freshening observed in surface sediments of the Anaximander Mountain area. Multiple fluid sources and formation water temperatures of 55 to 80 °C were derived for expelled fluids of the Olimpi area.

Keywords: mud volcano; cold seep; advection; bioirrigation; subsurface

1. Introduction

Submarine fluid flow and associated cold seeps have been found at various tectonically active and passive continental margins: well-studied active margin settings are the Cascadian (Kulm et al., 1986; Suess et al., 1999), the Aleutian (Suess et al., 1998), the Sagami (Masuzawa et al., 1992), the Nankai (Le Pichon et al., 1992; Henry et al., 1992), the Barbados (Henry et al., 1996), and the Costa Rica (Zuleger et al., 1996) subduction zones. Seepage along major fault zones is found off Monterey (U.S.A.) (Barry et al., 1996). Cold seeps at passive margins are mostly associated with rapidly accumulating sediments such as in the Gulf of Mexico (MacDonald et al., 1994), in the North Sea (Hovland et al.,

* Corresponding author. Present address: Geoscience Australia, P.O. Box 378, Canberra, ACT 2601, Australia.
E-mail addresses: ralf.haese@ga.gov.au (R.R. Haese), chensen@ifm-geomar.de (C. Hensen), gdelange@geo.uu.nl (G.J. de Lange).

0025-3227/$ - see front matter © 2005 Elsevier B.V. All rights reserved.
doi:10.1016/j.margeo.2005.09.001

1987) and on the Norwegian shelf (Ginsburg et al., 1999). If subsurface fluids become over-pressured, sediment is mobilized and subjected to expulsion at the sediment surface inducing mud flows and the build-up of mud volcanoes (Brown, 1990). The chemical composition of the expelled fluids can be used to deduce their origin with respect to the temperature conditions and the geologic regime (Dia et al., 1999). The depth distribution of pore water constituents allows to derive estimates of the advective flow velocity (Han and Suess, 1989; Wallmann et al., 1997). Advective flow rates at submarine seeps have been found to vary by four orders of magnitude (Moore and Vrolijk, 1992) which points to significant differences in the hydrodynamic conditions. Consequently, a distinction between diffuse and focused flow has been suggested.

Fluid seepage may be spatially and temporally highly variable on a local and regional scale. Consequently, estimates on the importance of cold seeps for global biogeochemical cycles are ambiguous. The volume of global annual fluid expulsion at cold seeps has been cautiously estimated to be 1 km^3 (Von Huene and Scholl, 1991). Boron (B) has been found to be significantly enriched in cold seep fluids and has consequently been included in an oceanic B budget (Lemarchand et al., 2000).

Ascending fluids are typically rich in methane, which is the basis for abundant and highly specialized micro-, macro- and megafauna effectively altering the chemistry of the fluids. In methane-rich sediments, microbial consortia consisting of archaea and sulfate reducing bacteria carry out anaerobic oxidation of methane (Hinrichs et al., 1999; Boetius et al., 2000; Pancost et al., 2000), which results in the production of dissolved inorganic carbon and sulfide (Kulm et al., 1986; Masuzawa et al., 1992; Boetius et al., 2000). Aerobic methane and sulfide oxidation serve as energy sources for free living and symbiotic microorganisms hosted within macro- and megasized benthic organisms. The macro- and megafauna exchange their burrow water with oxygen-rich bottom water by bioirrigation, which has significant impact on solute transport and biogeochemical reaction rates (Haese, 2002). The depth-integrated rate of bioirrigation can be compared to the advective flow velocity, illustrating the relative importance of each fluid transport mode at cold seeps (Wallmann et al., 1997). Apart from microbiologically mediated methane oxidation, methane may become stored in gas hydrate under certain temperature and pressure conditions and provides supersaturated concentrations of methane (Brooks et al., 1984; Haese et al., 2003).

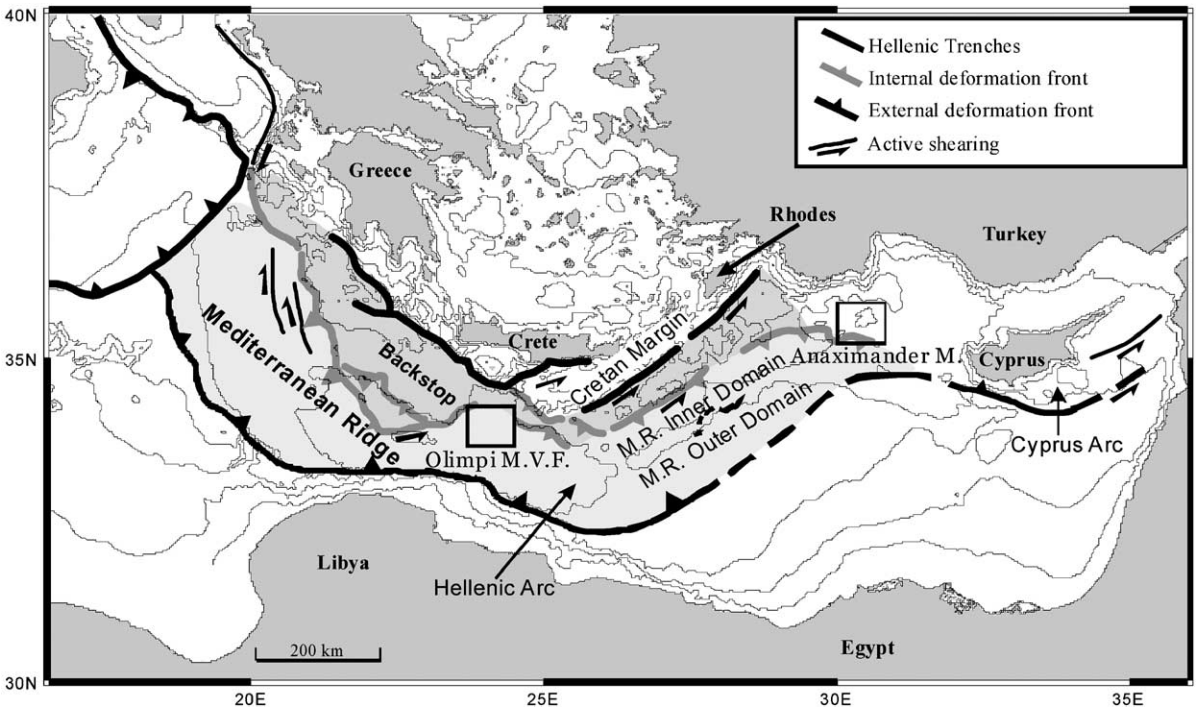

Fig. 1. Map of the eastern Mediterranean Sea with major tectonic units and the sampling areas (in boxes), the Olimpi Mud Volcano Field and the Anaximander Mountains (modified after MEDINAUT/MEDINETH Shipboard Scientific Parties 2000).

In this study sediments from eastern Mediterranean mud volcanoes located in the Olimpi Mud Volcano Field (Olimpi MVF) and the Anaximander Mountains (Fig. 1) are studied to better understand fluid transport and fluid origin at cold seeps. Estimates of advective flow velocities and rates of bioirrigation are derived from best-fit numeric simulations to measured depth profiles of conservative solutes (Na, B). The underlying assumption of steady state for such calculations is assessed by simulating the pore water re-equilibration after a major perturbation. Formation water temperatures of cold seep fluids are calculated using the chemical composition of major cations (Na, K, Mg) according to Giggenbach (1988). Whether or not solutes in the ascending fluids have been involved in reactions is tested and possible subsurface reactions are discussed.

2. Geologic setting and sampling sites

The Mediterranean Ridge is considered as a large accretionary complex extending for over 1500 km along the Hellenic Arc (Fig. 1). Over 150 circular to sub-circular high backscatter patches have been found by sidescan sonar along the Mediterranean Ridge and were identified as mud volcanoes or mud ridges mostly associated with thrust structures (Fusi and Kenyon, 1996). One of the prominent mud volcano fields of the Mediterranean Ridge is the Olimpi MVF south of Crete. Northeast of the Mediterranean Ridge lies the Rhodes Basin with the Anaximander Mountains adjoining further to the east (Woodside et al., 1998). The Anaximander Mountains form an area of pronounced seafloor relief which comprises mud volcanoes and escarpments with evidence of active fluid seepage (MEDINAUT/MEDINETH, 2000).

The formation of the Mediterranean Ridge is related to the ongoing collision between the African and Eurasian plates, which started in the Oligocene and has resulted in intensive folding and faulting. Lateral tectonic compression gives rise to stacking of sediment strata and deep fluid flow along fault planes (Limonov et al., 1996). The MEDRIFF and IMERSE programs (Westbrook and Reston, 2002) established the structure of the Mediterranean Ridge through NE–SW seismic transects in the western part of the Mediterranean Ridge: according to Fruehn et al. (2002) a 200–300-m-thin layer of Plio–Quaternary sediments is underlain by Messinian deposits with evaporites up to 3 km thick within basins, but evaporites were also found to be absent in intervening regions including the crest. Beneath the Messinian deposits, Tertiary clastic deposits are thinning towards northeast related to significant compaction form the growing wedge. In between the highly compacted Tertiary sediments and the top of the oceanic crust at a depth of approximately 10 km a 2.5 km thick layer of probably Mesozoic carbonate is located. Because the evaporites form an almost impermeable cap above the compacted Tertiary sediments, fluids become highly over-pressured, and the base of the Messinian section forms the basal decollement (Fruehn et al., 2002). PRISMED and PRISMED 2 initiatives provided insights into the structural setting of the eastern Mediterranean Ridge through seismic transects and swath mapping. An intensively folded outer Mediterranean Ridge domain in south was distinguished from an inner domain in the north (Fig. 1). The inner domain is characterized by giant mudflows and argilo-kinetic domes within a relatively low-topography terrain (Huguen et al., 2001). In the strongly folded outer domain, sediments of Pliocene to Quaternary age reach a thickness of 2 km and are underlain by 7 km thick Messinian evaporites.

The Anaximander Mountain area is located at the junction of the Hellenic and Cyprus arcs (Fig. 1) and consists of several sub-units: the most western part, the Anaximander Mountains s.s. (sensu stricto), is separated from the Anaximenes Mountains in the south and the Anaxagoras Mountains in the east through the Great Slide, an internal basin with mass flow infilling. The Anaximander Mountain area is structurally complex, and two zones are lithologically and structurally distinct (Ten Veen et al., 2004): The western mountains (Anaximander Mountains s.s. and Anaximenes Mountains) relate to neritic limestones of the Bey Daðlari unit of SW Turkey, while the eastern Mountains (Anaxagoras Mountains) belong to the ophiolitic Antalya Nappe Complex. The two mud volcanoes investigated in this study, the Amsterdam mud volcano and the Kazan mud volcano, are located at the SE edge of the Anaximenes Mountains and at the interception of the Anaximes and Anaxagoras Mountains, respectively. The Kazan mud volcano is transected by at least six fault orientations, which reflects the complex tectonic setting where the mud volcanoes are formed (Ten Veen et al., 2004).

3. Materials and methods

Here we report results from two expeditions. In 1998 the MEDINAUT scientific party explored with the French submersible *Nautile* the Olimpi MVF as part of the Mediterranean Ridge and the mud volcano field located in the Anaximander Mountains (Fig. 1). In 1999 the MEDINETH shipboard scientific party returned to both areas and sampled from board of *R/V*

Prof. Logachev by means of box, gravity and piston coring (MEDINAUT/MEDINETH Shipboard Scientific Parties, 2000). From the Olimpi MVF, submersible-operated push cores M-1 and M-2 and shipboard-operated gravity cores M-3 and M-4 were retrieved from Milano mud volcano and piston core N-1 was taken at Napoli mud volcano. Cores K-1, K-2, and K-3 are gravity cores, piston cores and box cores, respectively, from Kazan dome and gravity core A-1 was sampled at Amsterdam dome. Kazan and Amsterdam dome are mud volcanoes of the Anaximander Mountains. An overview of cores with their respective positions and water depths is given in Table 1.

3.1. Pore water extraction

Cores from the MEDINAUT expedition were sliced horizontally into segments of 0.5 to 2.5 cm under oxygen-free conditions in a glove-box at 14 °C (bottom water temperature) where pore water was extracted by pressure-filtration with N_2-pressure of up to 10 bars according to de Lange (1992). For gravity cores taken during the MEDINETH expedition, efforts were taken to minimize the time of core retrieval and sampling: The ship's winch for core retrieval was run with a velocity of approximately 120 m per min, which is about twice as fast as normal. The liner of the gravity core was a plastic foil, which was pulled out and opened lengthwise on the working deck within 1–2 min, cut-off syringes were pushed into the sediment and sealed with gas-tight tape. All syringe samples were subsequently transferred into centrifuge cups with screw caps. Each piston core was cut into pieces of approximately 1 meter, which were stored for no longer than 2 h at 5 °C prior to sampling. Rectangles of 5 cm^2 were sawed into the PVC liner through which samples were taken by cut-off syringes. A sub-core of the box core was transferred rapidly to a container with a temperature of 14 °C where the sediment was rapidly segmented under air, i.e. each sample was exposed to air less than 1 min, and transferred into centrifuge cups. Samples were centrifuged at 4000 rpm over 20 min. Extracted pore water was filtered through 0.2 μm cellulose-acetate membrane filters and sub-sampled for the various analysis under N_2-atmosphere.

3.2. Chemical analysis

Dissolved inorganic carbon (DIC) and salinity were measured on-board immediately after pore water extraction and filtration. DIC was analysed spectrophotometrically by a continuous flow set-up (Stoll et al., 2001). Interference from sulfide was avoided by the addition of H_2O_2. In view of the sampling procedure and the relatively high DIC concentrations, DIC concentrations must be considered as minimum amounts. Salinity was measured using a Reichart® refractometer. Because salinity is usually measured as grams per grams, salinity is here reported without unit, e.g. 36 rather than "36 PSU" or "36 [‰]".

Untreated pore water samples were stored at 14 °C (bottom water temperature) prior to dilution to a salinity of 3–4. From diluted samples Cl was measured by ion chromatography (Dionex®), and Na, B, K, Mg, and Ca were measured by ICP-AES at Utrecht University. DIC, Cl and ICP-AES standards were regularly measured as samples and showed a precision better than 4% for all methods.

Porosity was calculated from the loss of water after freeze-drying of the sediment. A mineral density of 2.6 g cm^{-3} was assumed.

4. Results

4.1. Major components (Cl, Na, Ca, Mg, K) and salinity

In Fig. 2 depth profiles of Na, B, and salinity are shown for all studied cores. Na and salinity run closely

Table 1
Locations, water depths (meters below surface, mbsl) and the associated mud volcanoes of the sampling sites

Original core code	Used code	Mud volcano	Location (Lat.; Long.)	Water depth (mbsl)
MN05CT1	M-1	Milano	33° 43.888′; 24° 46.674′	1961
MN17CT1	M-2	Milano	33° 43.927′; 24° 46.650′	1958
MNLGC01	M-3	Milano	33° 44.395′; 24° 46.740′	1951
MNLGC02	M-4	Milano	33° 44.406′; 24° 46.537′	1964
MNLPC03	N-1	Napoli	35° 20.013′; 30° 15.948′	1995
MNLGC07	K-1	Kazan	35° 25.941′; 30° 33.729′	1674
MNLPC10	K-2	Kazan	35° 25.950′; 30° 33.710′	1672
MNLBC19	K-3	Kazan	35° 25.936′; 30° 33.704′	1673
MNLGC11	A-1	Amsterdam	33° 43.546′; 24° 41.237′	1910

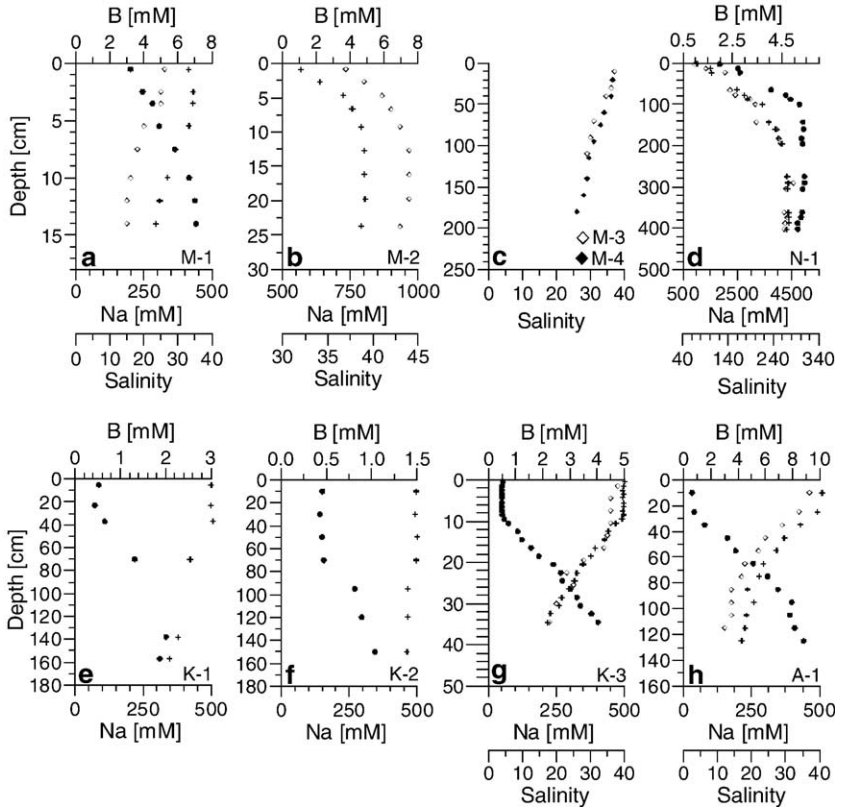

Fig. 2. Depth profiles of the conservative constituents B (dots) and Na (diamonds), as well as of salinity (crosses). Cores originate from Milano (a, b, c), Napoli (d), Kazan (e, f, g) and Amsterdam (h) mud volcanoes. Notice the differences in depth and concentration scales. Pore water freshening is indicated in case of reduced concentrations of Na relative to sea water (480 mM) and is typically associated with a top layer of rather invariable pore water concentrations.

parallel in the depth profiles. Interestingly, in cores from Kazan, Amsterdam and partly from Milano dome Na and salinity decrease with depth whereas in cores from Napoli and partly from Milano dome they increase. In contrast, B always increases with depth.

For Milano dome, a map is compiled distinguishing sites with increasing and decreasing Na concentrations with depth (Fig. 3). No systematic variation related to the distance from the center of the mud volcano can be seen. In contrast, at the summit of Milano dome the

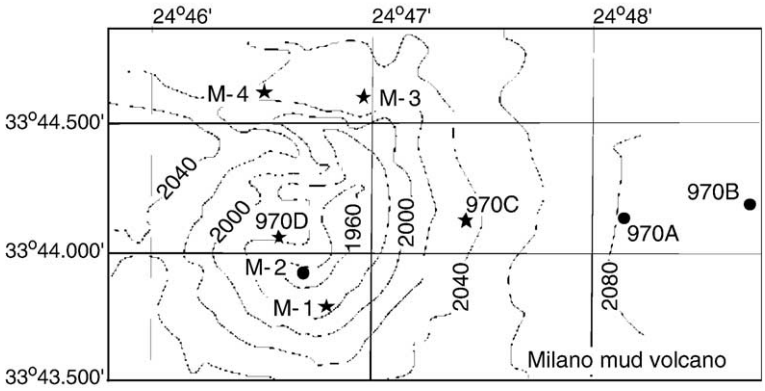

Fig. 3. Location map of cores retrieved from Milano mud volcano. See page of fluids with a higher salinity than sea water (dots) are spatially closely associated with seepage of fluids with reduced salinity (stars). Data from cores ODP 970A/B/C/D were adopted from de Lange and Brumsack (1998).

pattern of the salinity depth distribution is reversed within a 500-meter distance. Also, Na and salinity increase (M-2) and decrease exponentially (M-1) at the summit, whereas they decrease linearly with depth and essentially with the same gradient at the flanks of Milano dome (M-3, M-4). In contrast to the varying pattern in Na concentration and salinity, B always becomes enriched with depth relative to sea water on Milano dome.

Na concentrations and salinity in the Anaximander Mountain area always decrease with depth, whereas those of B always increase with depth. The change in concentration, however, always occurs below a surface layer of rather homogeneous composition. This layer typically extends to a depth of approximately 20 centimeters. In one case, however, it reaches down to 70 centimeters (K-2). Similar observations have been made at the Cascadia continental margin (Han and Suess, 1989), and at the eastern Aleutian subduction zone (Wallmann et al., 1997).

Groups of fluids with different chemical composition can be easily distinguished by correlations. Here,

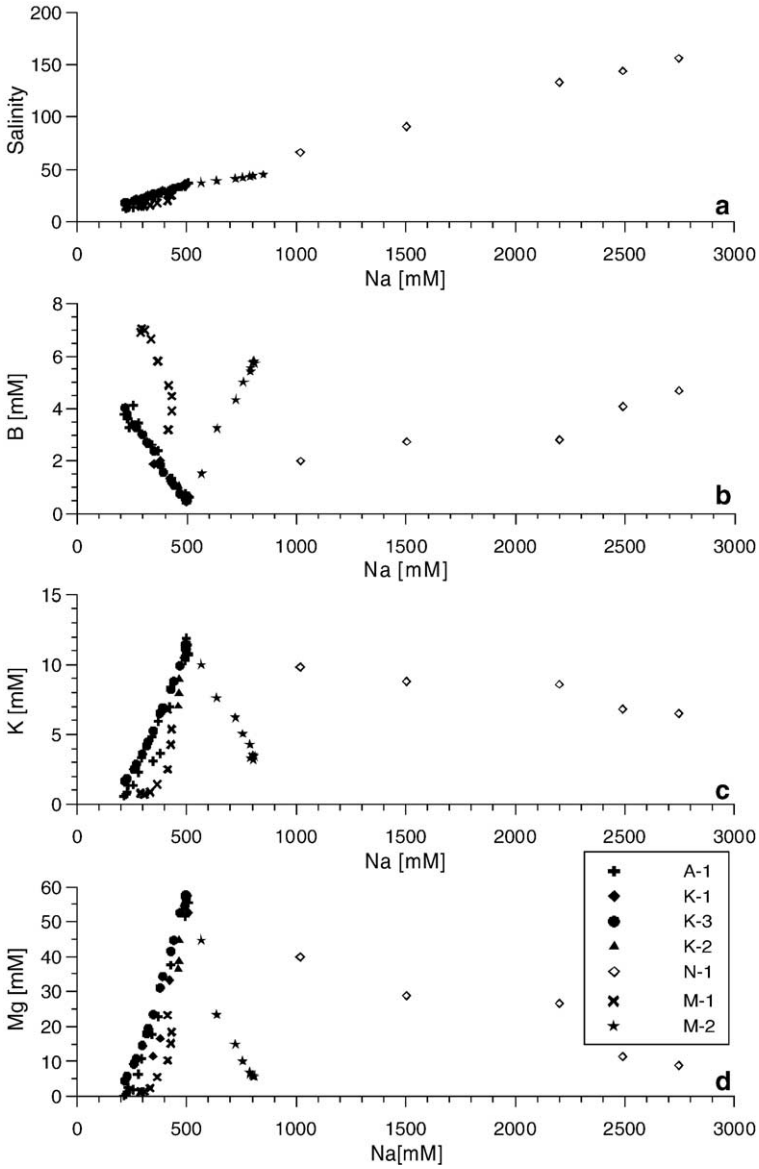

Fig. 4. Graphical correlations of Na with salinity (a), boron (b), potassium (c), and magnesium (d). Except for core M-1 linear correlations are observed illustrating a conservative behavior of the constituents in surface sediments. Sites with hypersaline fluids (M-2, N-1) are identified by increased Na concentrations relative to sea water (480 mmol l^{-1}).

Na is correlated with salinity, B, K, and Mg (Fig. 4 a–d). The salinity depth profiles already show the occurrence of two principal groups of ascending fluids, one having higher salinities and one having lower salinities than normal sea water. The solute correlation plots additionally reveal compositional differences within each major group. Within the group characterized by increased salinity, Milano site M-2 is much more enriched in B and depleted in K and Mg relative to Na than at site Napoli N-1. Similarly, within the group of fluids with reduced salinities, site M-1 is characterized by enriched B and depleted K and Mg concentrations relative to Na at the other sites (A-1, K-1, K-2, K-3). Na is in all cores by far the most abundant cation and its anionic counterpart is Cl (Table 2). For the two sites characterized by increased salinity, M-2 and N-1, Na/Cl-molar ratios are 1.00.

In order to estimate advective flow velocities and rates of bioirrigation from pore water profiles without including a reaction rate (Section 5.3) it is required to demonstrate a conservative behavior of the used constituents within the studied sediment interval. Conservative behavior is proven, if linear correlation between two solutes is given. This holds true for Na, B, K, and Mg in all cores, except in core M-1. Graphical correlations of core M-1 are concave-shaped (Fig. 4b–d), which is also reflected in the asymmetrical depth distribution of B and Na concentrations (Fig. 2a). Consequently, core M-1 will not be used to constrain an advective flow velocity and a rate of bioirrigation.

Na, Ca, Mg, and K concentrations are frequently used in geothermal studies to derive the temperature of the formation water (Giggenbach, 1997). Based on temperature-dependent equilibria between the fluid composition and major minerals of the average continental crust such as Na- and K-feldspar, smectite, illite, chlorite, and calcite, theoretical geothermometers have been developed. Here we apply the three independent theoretical geothermometers introduced by Giggenbach (1988). The geothermometers are based on the K–Na, K–Mg, and K–Ca composition of the sample:

$$T[^{\circ}\mathrm{C}] = \frac{1390}{1.75 - \log \frac{c(\mathrm{K}^+)}{c(\mathrm{Na}^+)}} - 273.15 \quad (1)$$

$$T[^{\circ}\mathrm{C}] = \frac{4410}{14.0 - \log \frac{c^2(\mathrm{K}^+)}{c(\mathrm{Mg}^{2+})}} - 273.15 \quad (2)$$

$$T[^{\circ}\mathrm{C}] = \frac{\log \frac{c^2(\mathrm{K}^+)}{c(\mathrm{Ca}^{2+})} + 0.78}{0.0168}. \quad (3)$$

All concentrations are given in mg/l.

For the reconstruction of the formation water temperature at cold seeps fluid samples with a composition closest to the original ascending fluid are chosen (Martin et al., 1996). This is typically the deepest sample in a core, because ions relatively enriched in the ascending

Table 2
Concentrations of major and minor constituents of samples from the lower end of the cores

Core	Depth (m)	Na	Cl	Ca	Mg	K	DIC	B	K/Na (°C)	K/Mg (°C)	K/Ca (°C)
K-3	0.35	218	267	0.67	4.41	1.66	15.78	4.03	109	82	177
K-2	1.50	463	550	4.51	36.56	7.02	7.71	1.04	143	92	202
K-1	1.60	348	536	4.86	11.52	3.12	3.64	1.88	116	86	158
A-1	1.25	145	248	0.33	0.16	0.59	25.28	3.79	82	98	142
N-1	4.00	4330	4338	0.54	5.23	5.43	52.74	5.41	n.a.	n.a.	n.a.
M-2	0.24	791	794	0.83	6.50	3.31	n.d.	5.42	n.a.	n.a.	n.a.
M-1	0.14	288	229	0.30	1.26	0.78	n.d.	6.91	67	79	159
ODP 970C*	970	315	350	0.53	2.07	0.77	n.d.	n.d.	63	73	144
ODP 970D*	41.8	146	88	b.d.l.	0.60	0.28	n.d.	n.d.	55	64	n.a.
ODP 971D*	45.35	3259	4074	b.d.l.	b.d.l.	4.07	n.d.	n.d.	n.a.	n.a.	n.a.
ODP 971E*	27.81	4100	5325	b.d.l.	b.d.l.	12.25	n.d.	n.d.	n.a.	n.a.	n.a.
Med. S.W.*		480	559	10.60	54.22	10.62	2.20	0.49	n.a.	n.a.	n.a.

All concentrations are reported in [mmol/l]. Formation water temperatures are calculated by three independent geothermometers according to Giggenbach (1988).
*: data from de Lange and Brumsack (1998).
b.d.l.: below detection limit.
n.d.: not determined.
n.a.: not applicable either because required concentrations were b.d.l. or fluids were hypersaline.
Med. S.W.: Mediterranean sea water.

fluid diffuse into the zone of bioirrigation or overlying bottom water, while ions relatively enriched in the top sediment diffuse downward along a concentration gradient. Wherever a constant value is reached at the lower end of a core, the chemical composition shows the closest approximation to the original fluid ascending from depth. Fluid samples from cores M-2, N-1, ODP 971D, and ODP 971E are excluded from geothermometry calculations because the high salinities indicate major evaporate influence in excess to the average continental crust.

The Na, Mg, K, and Ca concentrations used for the formation water temperature calculations and the respective results are given in Table 2. Overall temperatures range from 55 to 202 °C. The temperatures calculated with the K/Ca-geothermometer are consistently the highest, typically exceeding the K/Na and K/Mg thermometers by more than 50 °C. For the group of cores taken at Kazan mud volcano (K-1, K-2, K-3) formation water temperatures calculated with the K/Mg geothermometer are slightly lower than with the K/Na pair. Otherwise, calculated temperatures by the K/Na and K/Mg thermometers agree well with each other, showing temperature deviations less than 20 °C. K/Na and K/Mg temperatures calculated from fluids of Kazan (K-1, K-2, K-3) and Amsterdam (A-1) mud volcanoes are in the range of 80 to 145 °C, whereas the temperatures from Milano mud volcano (M-1, ODP 970C, ODP 970D) are significantly lower, varying between 55 and 80 °C.

The advantage of theoretical over empirical geothermometers is the option to check on the degree of equilibrium between the fluid and the host rock for the calculated temperature conditions. This is most easily accomplished by plotting major element data into a graph developed by Giggenbach (1988). In Fig. 5 one can see that all fluids analysed for the formation water temperature surround the line representing full equilibrium, which suggests that fluids have sufficiently reached the thermodynamic equilibrium with subsurface rocks to allow for the chosen approach.

4.2. B and DIC

B and DIC concentrations from the lowest sample of each core are enriched relative to seawater by up to more than one order of magnitude (Table 2). In Fig. 6, B versus DIC values from the eastern Mediterranean Ridge are plotted together with data of Dia et al. (1999) from Trinidad mud volcanoes and show a positive linear correlation with a similar slope. At first sight, this is a surprising finding, because DIC is formed by the process of anaerobic oxidation of methane, whereas

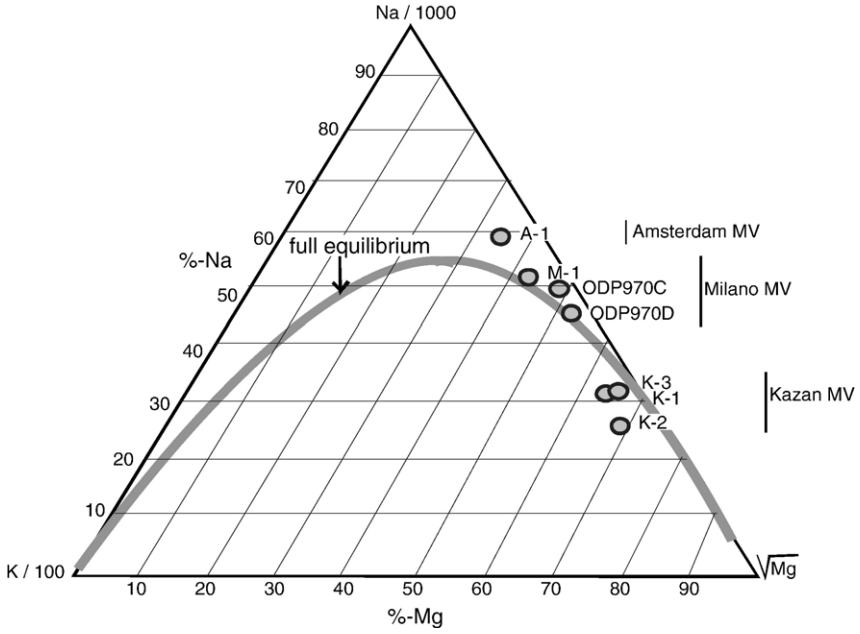

Fig. 5. Graphic representation illustrating the degree of equilibrium between the fluid chemistry and the host rock accounting for the in situ temperature (redrawn from Giggenbach, 1988). With: %-Na = C(Na)/10 S; %-Mg = 100 $\sqrt{C}$(Mg)/S; $S = C$(Na)/1000 + C(K)/100 + $\sqrt{C}$(Mg), and all concentrations in [mg l^{-1}]. The dots represent the composition of pore water samples from the lower end of cores to minimize the effect of mixing with sea water (see text).

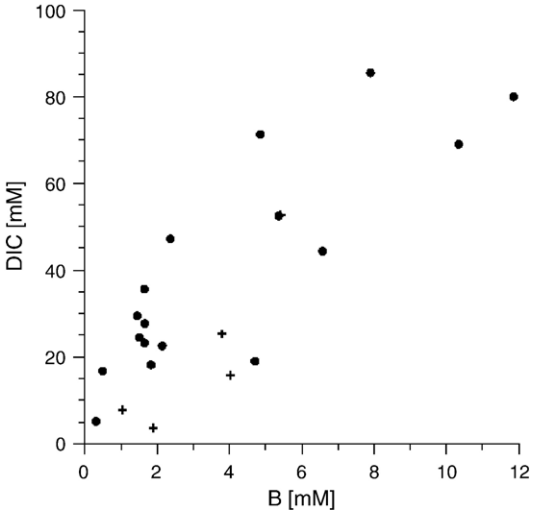

Fig. 6. Correlation between dissolved inorganic carbon (DIC) and boron (B) concentrations of samples from Trinidad mud volcanoes (dots, Dia et al., 1999) and from the deepest samples in cores retrieved from eastern Mediterranean mud volcanoes (crosses, Table 2). The linear correlation of all data has a correlation coefficient (r^2) of 0.7.

B behaves conservatively in surface sediments. However, the influence of anaerobic oxidation of methane on DIC concentrations is limited to the upper sediment interval. DIC concentrations gradients are steepest in a very narrow zone of anaerobic oxidation of methane and gradually decrease downward as a function of distance from the reactive zone (Fig. 7). The lowest sample of each core is apparently sufficiently deep, so that it is insignificantly affected by anaerobic oxidation of methane. The linear correlation of the two solutes will be discussed with respect to possible deep subsurface processes leading to contemporary enrichments (Section 5.2).

5. Discussion

5.1. Presence of gas hydrate

Information on the abundance of gas hydrate is essential for the interpretation of all pore water data because samples become exposed to decreasing pressure and increasing temperature conditions during core retrieval resulting in the potential dissociation of hydrate, which in turn leads to dilution of ambient pore water. Since sea floor pressure and temperature conditions of eastern Mediterranean mud volcanoes principally allow for the formation of gas hydrate with a stoichiometry of $CH_4 \cdot 6H_2O$ and pore water freshening had been observed before, abundant gas hydrate was predicted for the studied surface sediments (de Lange and Brumsack, 1998; MEDINAUT/MEDINETH Shipboard Scientific Parties, 2000). However, during the MEDINAUT and MEDINETH expeditions macroscopic-sized pieces of gas hydrate were only found at two sites, which are not discussed in this study.

The highest methane bottom water concentrations of Kazan mud volcano were found above site K-3 (149 nmol kg^{-1}, Charlou et al., 2003) and the respective DIC pore water gradient was the steepest in our data set (Fig. 7). These observations suggest, that site K-3 is one of the most active cold seep sites investigated during MEDINAUT/MEDINETH expeditions. Yet, at the same site gas hydrate is only stabilized below 2 meters of sediment depth (Haese et al., 2003), which implies that gas hydrate formation at other studied sites is likely to be restricted to depths even greater than 2 meters. Consequently, only insignificant amounts of gas hydrate are expected to be present in the studied cores as they are shorter than 2 meters, except for core N-1. The sample site of core N-1, however, is characterized

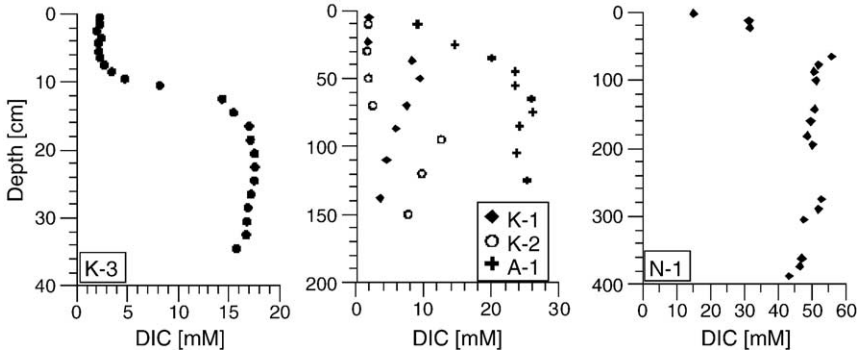

Fig. 7. Depth profiles of dissolved inorganic carbon (DIC) from three mud volcanoes (Table 1). Although DIC is formed by the process of anaerobic methane oxidation and consumed by carbonate precipitation in near-surface sediments an asymptotic concentration is reached with increasing depth. Deepest samples are regarded to resemble the original DIC concentration of the ascending fluid (Fig. 6). For core locations refer to Table 1.

by hypersaline fluids, where dilution from dissociating gas hydrate is not expected.

Pore water freshening resulting from dissociating gas hydrate has additionally been disproved based on the stable isotopic composition ($\delta^{18}O$, δD) of the fluids found at sites ODP 970 and ODP 971 (Dählmann and de Lange, 2003). The extent of the found ^{18}O enrichment and reduced δD values for fluids recovered during ODP drilling in eastern Mediterranean mud volcanoes suggest other reasons for pore water freshening than gas hydrate dissociation. A third line of reasoning comes from pore water concentration profiles of conservative constituents. Na and B, as well as salinity (Fig. 2) show very even and consistent depth distributions (Section 4.1). In contrast, it is known that abundant gas hydrate forms discrete layers (Suess et al., 1999), which is reflected by a scattering depth distribution of conservative constituents. For a quantification of gas hydrate in the well-studied sediments of Blake Ridge, the most recent interpretation of the chloride concentration profile has shown that the freshening from hydrate dissociation during sample retrieval contributes little to total freshening, i.e. less than 50% (Egeberg and Dickens, 1999). In summary, several lines of reasoning argue for the absence of significant quantities of gas hydrate within the studied cores. As a consequence, the observed freshening of pore water will be discussed below with respect to the origin of ascending fluids alone.

5.2. The origin of fluids

Two general types of seeping fluids can be distinguished on the basis of chlorinity. All cores from Napoli dome (N-1, ODP 971D, ODP 971E) and partly from Milano dome (M-2, ODP 970A, ODP 970B) (Fig. 2, Table 2) show Cl concentrations up to 9 times higher than sea water. This observation points to a major influence by salt deposits, which indeed are known to have formed during Late Miocene age and are found beneath the Olimpi MVF. The presence of these deep subsurface salts associated with the active accretionary prism give rise to the formation of submarine brine lakes in the area (de Lange and Ten Haven, 1983; Jongsma et al., 1983) with a chemical composition derived from highly evaporated, residual brines enclosed in salt deposits (Vengosh et al., 1998). The second type of seeping fluid is found at Kazan (K-1, K-2, K-3), Amsterdam (A-1) and partly at Milano dome (M-1, M-3, M-4, ODP 970C, ODP 970D) and is characterized by chlorinities lower than sea water (Table 2). The observed freshening of pore water will be discussed below in relation to expected fluid–rock interactions at their respective subsurface temperatures.

Subsurface temperatures from the depth of the fluid origin are estimated with the three independent equations (Eqs. (1) (2) and (3)) based on cation concentrations of representative samples (Section 4.1). Earlier comparisons of different equations estimating the formation water temperature have shown that significantly different temperatures may result. Particularly, equations accounting for the Ca concentration have revealed unreasonably high temperatures (Martin et al., 1996), which is also observed in this study (Tabel 2). Geothermometers based on the fluid Si content are ambiguous, because the mineral controlling the Si concentration is unknown. In this study Si concentrations in the deepest samples of the studied cores are too low to give reasonable formation water temperatures assuming equilibrium with quartz, chalcedony, or a-cristobalite (data not shown). Most likely, Ca and Si are involved in reactions while the fluid becomes exposed to reduced temperature and pressure conditions resulting in depleted concentrations relative to the original formation water.

Similar to the experiences with formation water temperature reconstructions at cold seeps by Martin et al. (1996), the most consistent and reasonable temperature reconstructions are achieved with cation geothermometers involving K, Na, and Mg. The combination of the latter three cations can also be used to assess the degree of equilibrium between the fluid composition and ambient rock at the reconstructed temperature. It is shown, that the used fluid samples are close to equilibrium (Fig. 5) validating the achieved results. Note, that sites with hypersaline seeping fluids have a priori been excluded from formation water temperature reconstruction (Section 4.1). Reconstructed temperatures based on the composition of K, Na, and Mg ions generally range from 55 to 145 °C. Ascending fluids at Kazan and Amsterdam mud volcanoes reveal relatively higher temperatures (80–145 °C), while temperatures reconstructed from fluids of Milano mud volcano are significantly lower (55–80 °C).

For Kazan mud volcano (K-1, K-2, K-3) the K–Mg temperatures are consistently and significantly lower than the K–Na temperatures. According to Giggenbach (1988) this can be explained by faster re-equilibration kinetics for the K–Mg pair in comparison to the K–Na pair. Thus, in the case of the Kazan temperature reconstructions the K–Na temperature is a better estimate for the original formation water temperature than the K–Mg pair. This implies that original temperatures are roughly between 100 and 150 °C for fluids from Kazan mud volcano. Calculated formation water tem-

peratures for Amsterdam (A-1) and Milano mud volcanoes (M-1, ODP 970C, ODP 970D) reveal only small differences (<20°C) between the K–Mg and K–Na pair methods, indicating that the fluids have retained their original K, Mg, and Na compositions and are in near-equilibrium with the surrounding mineral phases at the depth of fluid formation (Giggenbach, 1988). Therefore, the estimated formation water temperature for Amsterdam mud volcano is 80–100 °C and for Milano dome it is 55–80 °C.

A study on organic compounds and vitrinite reflectance of muds from the Olimpi MVF revealed two important information with regard to the origin of muds (Schulz et al., 1997): (i) accounting for a geothermal gradient between 20 and 30 °C/km (Camerlenghi et al., 1995), vitrinite reflectance data suggest a depth of mud mobilization between 4900 and 7500 m. The respective temperature at the depth of mud mobilization is then 100–120 °C. (ii) The muds contain organic matter of fresh- and brackish-water origin which agrees with the general Messinian depositional environment. Given the calculated formation water temperature for Milano seep fluids of 55–80 °C and a reconstructed temperature at the depth of mud mobilization of 100–120 °C, the depths of fluid and mud mobilization appear to be decoupled. This suggests that the present Milano seep fluid is mobilized from the interior of the accretionary wedge rather than from its base. Possibly, the subducted fresh- and brackish-water of Messinian origin is extruded from discrete non-evaporite layers in close proximity, but isolated from evaporite-containing strata. This would also explain the local nature of seepage and the high variability of seep fluid composition found on Milano dome (Fig. 3). Note, however, that the relatively shallow depth of fluid mobilization may be restricted to the present dormant phase of Milano mud volcano (Kopf et al., 1998). Once mud volcanism becomes active, one would expect that fluids and muds have a common source depth.

In the Anaximander Mountain area, reconstructed formation water temperatures of the Kazan mud volcano (100–150 °C) are distinctively higher than of the Amsterdam mud volcano (80–100 °C), which may be related to the regional structural setting. Kazan dome is located on top of the Bey Daðlari Unit which has deep cutting faults and is in close proximity to the Antalya nappes basement. In contrast, at the site of Amsterdam dome faults are shallower and basement rocks with a high geothermal gradient are not in near proximity (Ten Veen et al., 2004). Higher formation water temperatures at Kazan dome may thus be related to a greater depth of fluid formation and/or a greater geothermal gradient caused by the near-by basement crust.

The temperature range of 55 to 150 °C for formation waters expelled at eastern Mediterranean mud volcanoes is similar to temperatures of 70 to 150 °C determined for Trinidad mud volcanoes (Dia et al., 1999). Further similarities in chemical composition and the related origin of the fluids come from the linear positive correlation of B and DIC (Fig. 6). High B mobilization is well known in accretionary prisms (You et al., 1993) and is predominantly related to desorption from clay minerals (Brumsack and Zuleger, 1992). Overlapping with the temperature range where B is released, high concentrations of organic acids such as acetate have been observed in the Gulf of Mexico by Land and Macpherson (1992). In their extensive data compilation highest organic acid concentrations (up to 2 g/l as acetate) were found at around 100 °C. Organic acid depletion below 60 and above 140 °C was attributed to microbial and thermogenic decomposition, respectively. Consequently, the produced low molecular weight organic acids are likely to be microbially decomposed during the fluid ascent and cooling, e.g. by acetate fermentation, $CH_3COOH \rightarrow CH_4 + CO_2$ (e.g. Whiticar, 1999). Other fermentation processes may additionally contribute to the production of DIC. Reconsidering the positive correlation between DIC and B (Fig. 6) and the given temperature constraints on C and B biogeochemistry, we propose an increase of pore water B by desorption from clay minerals with contemporary DIC production via organic acid production and subsequent fermentation processes.

A subsurface temperature of 80 to 150 °C may not only have important implications for B and C (bio-) geochemistry in accretionary prisms but also for required physical conditions to form mud volcanoes and create fluid flow: The hydrous clay mineral smectite starts to release water by dehydration during the first stage of its transformation to illite at temperatures between 80 to 100 °C (Colten-Bradley, 1987). As a result, pure water dilutes ambient fluid. Smectite enriched sediment intervals are typically associated with seismic decollements in subduction zones presumably due to the transition from mechanically weak smectites to mechanically strong illites (Vrolijk, 1990). Consequently, the decollement serves mechanically as a shear plane and hydrologically it forms a major conduit due to the release of water and build-up of pressure (Gieskes et al., 1990; Moore and Vrolijk, 1992). These general considerations apply well to the Nankai and Barbados decollements, where temperatures of about 100 °C (Kastner et al., 1993; Gieskes

et al., 1993; Vrolijk, 1990) and B concentration of about 10 mmol l^{-1} (You et al., 1993) were found. Similar conditions are expected for the decollement of the eastern Mediterranean accretionary prism based on the calculated formation water temperatures of this study. This is supported by a recent study on the O and H stable isotope composition of fluids from the Olimpi MVF, which revealed smectite dehydration as prominent source for freshwater in the seep fluids (Dählmann and de Lange, 2003). Fluid freshening may be quantitatively significant as has been demonstrated by Morton and Land (1987). According to their results subsurface clay mineral dehydration may lead to chlorinities as low as 1/3 of normal sea water.

5.3. Modeling fluid transport

Before values for certain model variables are determined by finding the best-fit to measured results the relevant processes must be known and implemented into the used model. Molecular diffusion and fluid advection occur at cold seeps and their respective terms used in 1-dimensional transport models to quantify these processes have successfully been used (Han and Suess, 1989; Wallmann et al., 1997). These two processes, however, only explain the upward-curved lower part of the solute pore water profiles (Fig. 2). In order to explain the well-homogenized top layer in the pore water profiles an additional process must be taken into account.

In principle, gas ebullition, gravity driven mass flow, fluid convection and bioirrigation may lead to constant pore water concentrations in surface sediments. In this study, gas ebullition can be excluded, because gas bubbles escaping from the sediment have never been observed during the 20 dives with the submersible during the MEDINAUT expedition. Gravity driven mass flow resulting in the mixing of the surface sediment including the pore water (Hensen et al., 2003) can also be excluded in our study, because the studied mud volcanoes are typically pie-shaped sea floor features with relatively flat summit areas (MEDINAUT/MEDINETH shipboard parties, 2000) from where most cores were retrieved. A third alternative explanation for rather homogeneous pore water concentrations in the top sediment is fluid convection. Intense downward advection to a discrete depth could in fact result in the observed homogenized pore water surface layer similar in composition as sea water, but moderate to low downward advection velocities would result in a reversed curvature of the pore water profile in surface sediments as compared to a profile dominated by upward advection. Solute concentration profiles affected by upward advection are curved upwards, whereas concentration profiles affected by downward advection should be curved downwards. The latter is not observed in our study and has not been found elsewhere to our knowledge.

Alternatively, bioirrigation may lead to a homogenized pore water surface layer by sustaining the bidirectional exchange of fluid within burrows and tubes of macrobenthic infauna. Cold seeps are known as sites of abundant macro- and megafauna intimately associated with sulfide- and methane-oxidising symbiotic bacteria (Sibuet and Olu, 1998). In order to detoxify their adjacent environment and to supply the required oxygen for chemosynthesis to depths where sulfide and methane is abundant macroorganisms rapidly exchange their burrow water with oxygen-rich bottom water. Although, we do not have information on the abundance of infauna at the studied sites, their presence and the induced bioirrigation are likely, because the required geochemical conditions are given. Furthermore, abundant epifauna has recently been described for the studied areas (Olu-Le Roy et al., 2004). Consequently, bioirrigation is most likely the process resulting in the homogenized pore water surface layer, and as such it will be implemented in our model.

Na and B have been shown to behave conservative in the studied surface sediments (Section 4.1), i.e. these solutes do not undergo any reactions. Note, that the change in temperature with depth in these sediments is smaller than 0.2 °C/m (J.-P. Foucher, pers. comm.), which means that temperature induced fluid–rock interactions (e.g. You et al., 1996) can be excluded within the studied top 4 m of sediment. Similarly, Arnórsson (1985) found conservative behavior for Cl, Na, and B during mixing of hot and cold water within a geothermal system. Furthermore, Na and B were shown to behave conservative in the estuarine fresh- and marine water mixing zone (Savenko et al., 2002).

Under the assumption of conservative behavior of the observed constituents and constant porosity the depth distribution of a solute can be described with the following one-dimensional steady-state differential equation accounting for diffusion, advection and irrigation (e.g. Boudreau, 1997):

$$D_s \cdot \frac{\partial^2 C}{\partial x^2} + v \cdot \frac{\partial C}{\partial x} - \alpha_x \cdot (C_x - C_0) = 0 \qquad (4)$$

with v is the fluid advection velocity relative to the sediment surface, x is sediment depth, C is the concentration, α_x is the depth-dependent non-local mixing

Table 3
Model results for the advective flow rate, v, and the non-local mixing coefficient, α, derived by simultaneous fitting of the conservative constituents Na and B

Core	v (cm y^{-1})	α (y^{-1})	Depth of α (cm)	Depth-integrated α (cm y^{-1})
K-2	5	100	17–20	300
K-1	3	50	69–72	150
K-3	4	100	8–11	300
A-1	5	50	33–36	150
N-1	3	–	–	–
M-2	50	–	–	–

For applied boundary conditions see text. At the sites with seepage of hypersaline fluids, N-1 and M-2, no indication for bioirrigation was given.

coefficient, and $(C_x - C_0)$ is the difference between the concentration at any depth in the sediment and in bottom water. The effective diffusion coefficient in the sediment, D_s, was derived from the temperature corrected molecular diffusion coefficient (Li and Gregory, 1974), D_m, by accounting for the tortuosity of the sediment, θ, according to $D_s = D_m/\theta^2 \cdot \theta^2$ was calculated by $\theta^2 = 1 - \ln(\phi^2)$ according to Boudreau (1997). ϕ represents the porosity of the sediment.

As compared to a previous study in which only advective flow velocities were calculated for cores K-1, K-2, and K-3 (Haese et al., 2003) the used differential equation in this study includes a term for bioirrigation (Eq. (4)). In practice, we made use of the coupled transport and reaction model CoTReM, which is capable to compute one-dimensional pore water profiles by accounting for the used transport processes and reactions. A full description of the model CoTReM is given elsewhere (Adler et al., 2001; Pfeifer et al., 2002). Boundary conditions were set as follows: concentrations at the upper and lower boundary of the model column were set to measured data values. α was implemented over a depth interval of 3 centimeters for cores A-1, K-1, K-2, and K-3 at the interface separating the top layer of rather homogeneous pore water composition from the zone below (Table 3). Since CoTReM is a non-steady state model the run time of the model was determined by the time of reaching a quasi steady state. Best-fit simulations for Na and B were achieved by varying α and v simultaneously for both constituents and are shown in Fig. 8.

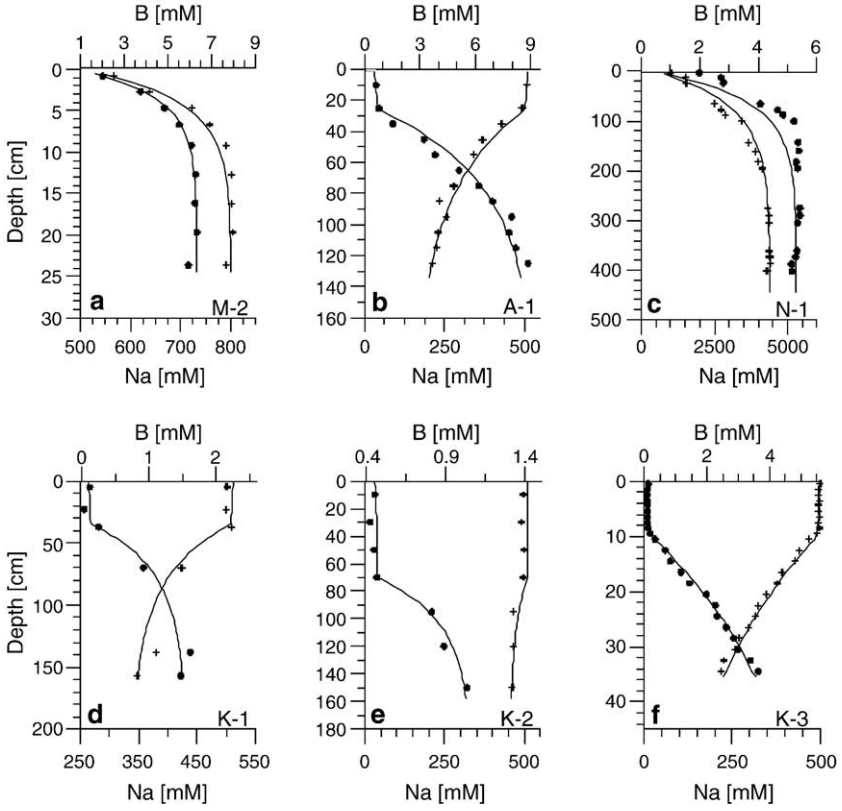

Fig. 8. Model results (solid lines) achieved from simultaneous fitting of Na (crosses) and B (dots) according to the mass conserving transport equation (Eq. (4)) accounting for diffusion, advection and bioirrigation. Fitting procedure is described in the text and best-fit parameters (advection velocity (v) and bioirrigation coefficient (α)) are listed in Table 3. For core locations refer to Table 1.

Advection velocities (Table 3) for the cores taken without visual control are very similar, varying between 3 to 5 cm y^{-1}. In contrast, the fluid advection velocity derived from a core taken with the submersible *Nautile* (M-2) is one order of magnitude higher (Table 3). The latter core was taken on the basis of visible indications such as abundance of biota, rough surface topography and dark grey patches, which confirms the assumption that visible indicators indeed reflect increased seeping activity.

Advective flow velocities of 4 ± 1 cm/y were earlier derived independently of bioirrigation for the three cores from Kazan mud volcano (K-1, K-2, K-3) (Haese et al., 2003). These earlier results agree very well with results of this study (Table 3), which relates to the fact that the lower boundary of the bioirrigation zone is treated as the upper boundary of the zone, where only molecular diffusion and advection are effective. The calculated advective flow velocities derived from cores taken without visual control compare well with flow rates determined with the same approach at Cascadia margin (1–28 cm y^{-1}; Han and Suess, 1989). In contrast, flow rates at Cascadia margin were 2 to 4 orders of magnitude higher (30 to 1065 m y^{-1}) at sites selected by eye (Linke et al., 1994).

Irrigation is expressed as non-local mixing, α, over the total irrigated zone in case of a narrow zone of fluid mixing or over the lowermost depth interval (3 cm) in case of a broad bioirrigation zone (>10 cm). This distinction is made to account for the ecological conditions at cold seeps, which typically restrict the diversity of the large infauna to very few species living at discrete sediment depths. All cores with an indication for bioirrigation were taken without visual control and consequently no information on the seep fauna specifically at the sampling sites can be provided. However, only recently a study on seep macrofauna communities of the Olimpi MVF and the Anaximander Mountains was published (Olu-Le Roy et al., 2004): it is shown that lucinid bivalves, particularly *Myrtea* sp., are most abundant. Small vesicomyid and mytilid bivalves and tube worms, e.g. *Lamellibrachia* s., were also frequently found. Dense bivalve shell accumulations were found to cover 10%–38% of the explored areas suggesting seep communities are generally widespread. Well known contributors to bioirrigation at cold seeps are bivalves such as *Calyptogena* sp. and *Solemya* sp. (Wallmann et al., 1997).

Best-fit derived non-local bioirrigation coefficients vary between 50 and 300 y^{-1} (Table 3). α-values are additionally integrated over the depth interval of non-local mixing resulting in a flow velocity, e.g. across the sediment/water interface. This value can be compared to the prevailing advective flow velocity as well as to results of other studies where α is kept constant over the total zone of bioirrigation. Our results demonstrate that fluid transport induced by bioirrigation (150–300 cm y^{-1}) exceeds physically driven advective flow (3–50 cm y^{-1}) by 1 to 2 orders of magnitude at the studied sites of the eastern Mediterranean Sea (Table 3). Similarly, at a very active cold seep site of the Aleutian margin depth-integrated bioirrigation was found to be higher (900 cm y^{-1}) than the advective flow velocity (340 cm y^{-1}; Wallmann et al., 1997).

5.4. Testing the assumption of pore water steady state

Mud volcanoes are formed by a succession of sporadic eruptions of fluidized mud over millions of years and consequently, surface sediments are exposed to temporary perturbations. For the model calculations resulting in estimates of advective flow velocity and rates of bioirrigation (Section 5.3), steady state with regard to the pore water profiles of conservative solutes has been assumed. In this section we test the assumption of steady state in a mud volcano environment by simulating the post-depositional evolution of the conservative solutes Na and B after the deposition of a 2-meter thick mud deposit. Such mudflow events are reasonable as no transition from one mud deposit to another is observed in the sedimentological descriptions of the cores.

The model runs are stopped after chosen time intervals prior to reaching steady state. The initial mudflow fluid composition is assumed to be uniform and equal to present-day pore water composition measured at depth (Table 2). Since information on the temporal changes in porosity, bioirrigation and advective flow velocity subsequent to the simulated perturbation can not be constrained, the three variables are kept constant with time using values derived in Section 5.3 (Table 3) for the sites K-1 and M-2.

The results of the transient state simulations are displayed in Fig. 9. Steep gradients between the bioirrigated zone and the underlying sediment develop on a time scale of 1 to 12 months due to intense bioirrigation. The pore water gradients then decrease with time and reach quasi steady state within 10 to 30 years in case of a low advective flow velocity (3 cm y^{-1}, K-1). When a moderate advective flow velocity is used and bioirrigation is excluded (50 cm y^{-1}, M-2), a new steady state is reached within months. Compaction effectively enhances the advective flow velocity, which would result in even shorter pore water re-equil-

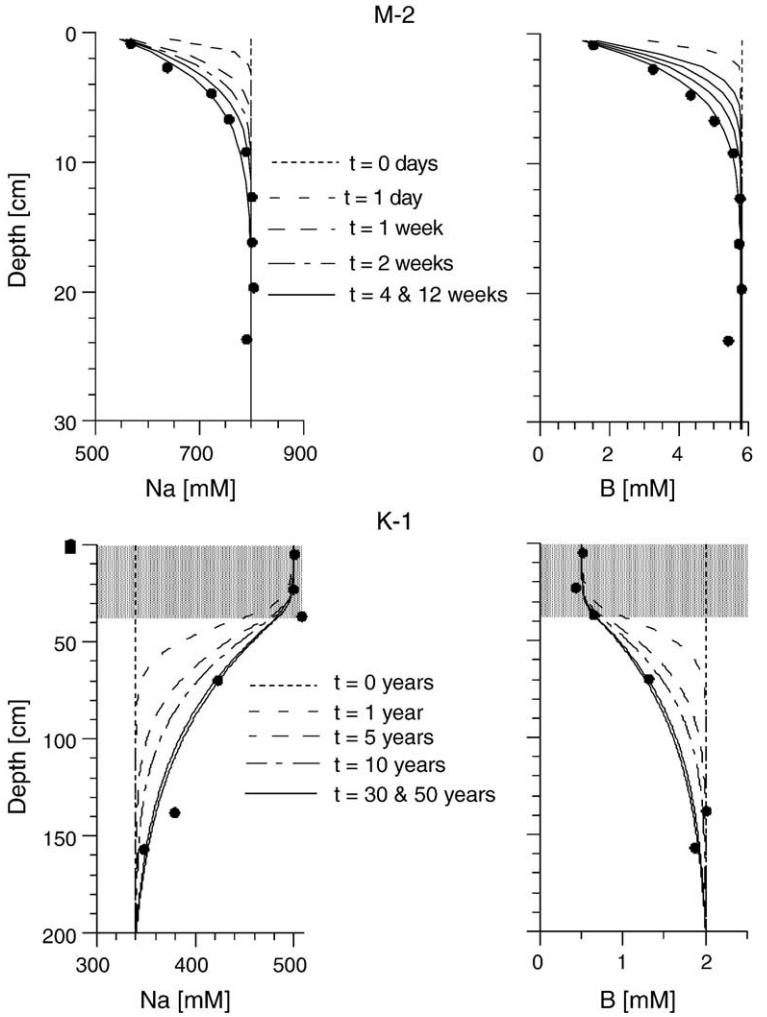

Fig. 9. Results of pore water simulations estimating the period of non-steady state after the deposition of a massive mud flow, e.g. thicker than 2 meters. Constant advective flow velocities of 50 and of 3 cm y^{-1} are assumed for sites M-2 (Milano MV) and K-1 (Kazan MV), respectively (Table 2). At site K-2 bioirrigation in the top 35 cm (grey shaded zone) is additionally accounted for (Table 3). For further boundary conditions and variables see text. Within months (M-2) to several tens of years (K-1) a new steady state is reached under the described conditions.

ibration times. Consequently, approximately 10 years is a conservative estimate for a non-steady state period after a major perturbation such as the deposition of a massive mud flow.

The frequency of mud deposition events can be roughly estimated from the finding of several centimeter thick intercalated pelagic sediment and decimeter thick intervals of oxidised, yellow-light brown colored mud breccia intervals as found on top of core K-1. At the given pelagic sedimentation rate of 4 cm ky^{-1} in the eastern Mediterranean Sea, unperturbated periods by the order of 1000 years can be assumed, if intercalated pelagic sediment of a few centimeter thickness is found. Studies on the downward progression of oxygen ('burn-down') in turbidites that are poor in organic matter have shown that decimeter-deep oxygen penetration is accomplished within 100 and more years (Wilson et al., 1986). When additionally accounting for the oxidation of methane and/or sulfide by oxygen driven by the high fluxes of these reduced species (Haese et al., 2003), the required time for oxygen to penetrate into mud volcano sediment will be significantly longer than in turbidite sediments. In summary, the sedimentological indications argue for a mud deposition frequency typically on the order of 1000 years. When periods of non-steady state (~10–30 years) are compared to unperturbated periods (~1000 years), the assumption of pore water steady state is justified for most cases.

6. Conclusions

Formation water temperatures between 55 and 145 °C were derived for the seeping fluids of eastern Mediterranean mud volcanoes, which is in agreement with previous studies on accretionary prisms and has important implications for deeper subsurface processes. Smectite transformation into illite is expected to occur in the deeper subsurface with concurrent release of intercrystalline water, which leads to the observed pore water freshening in surface sediments. Significant pore water freshening from gas hydrate dissociation during core retrieval is unlikely in the studied areas. A reasonable correlation between DIC and B enrichments in the ascending fluids was found suggesting that subsurface fermentation and B desorption from clay minerals take place concurrently during fluid formation and advection. However, carbonate precipitation must be accounted for as a secondary reaction involving DIC, which may explain the unreasonably high formation water temperatures calculated with the K–Ca geothermometer as compared to the consistent temperature range calculated with the K–Na and K–Mg geothermometers.

Typically, fluid advection in surface sediments is a few centimeters per year, which is generally low to moderate compared to other reported cold seep sites. The deposition of a massive mud flow is considered as one possible major perturbation of surface sediments and its pore water. Simulations, however, demonstrate that only very short non-steady state periods during pore water re-equilibration (10–30 years) prevail relative to steady state (1000 years) periods. The spatial heterogeneity in the hydrology of eastern Mediterranean cold seeps is particularly reflected in the chemistry of seeping fluids. On Milano mud volcano fluids with enriched and depleted salinities relative to sea water are found only 500 meters apart from each other. This implies that multiple sources of fluids and their respective discrete pathways of fluid transport may feed cold seeps of one mud volcano.

The observed homogeneous pore water surface layer typically extends down to a depth of 20 centimeters and is explained by intense bioirrigation. Depth-integrated bioirrigation coefficients turn out to be 1 to 2 orders of magnitude higher than the moderate advective flow velocities. Consequently, benthic fluxes and surface sediment reaction rates are expected to be strongly enhanced by the activity of cold seep macro fauna as has been found elsewhere. A relationship between the flux of reduced species (sulfide and methane) driven by advection and bioirrigation activity seems plausible, but remains to be fully explored.

Acknowledgements

We thank the captains and the crews of research vessels *Logachev* and *Nadir*, the *Nautile* technicians, and J. Schilling and W. Polman (NIOZ) for their assistance and dedicated cooperation. K. Bakker (NIOZ), G. Nobbe and T. van Wijk (University Utrecht) are thanked for their analytical work. The comments by the editor and two anonymous reviewers very much improved the manuscript. Funding was received from the Dutch science foundation (NWO) for the MEDINETH (750.199.01) and the SMILE program (750.297.01C). Additional support was obtained by the European Union Marine Science and Technology Program, contract number MAS3-CT97-0137. This manuscript represents NSG publication number 20010802.

References

Adler, M., Hensen, C., Wenzhöfer, F., Pfeifer, K., Schulz, A.D., 2001. Modeling of calcite dissolution by oxic respiration in supralysocline deep-sea sediments. Mar. Geol. 177, 167–189.

Arnórsson, S., 1985. The use of mixing models and chemical geothermometers for estimating underground temperatures in geothermal systems. J. Volcanol. Geotherm. Res. 23, 299–335.

Barry, J.P., Greene, H.G., Orange, D.L., Baxter, C.H., Robison, B.H., Kochevar, R.E., Nybakken, J.W., Reed, D.L., McHugh, C.M., 1996. Biologic and geologic characteristics of cold seeps in Monterey Bay, California. Deep-Sea Res. (I) 43, 1739–1762.

Boetius, A., Ravenschlag, K., Schubert, C.J., Rickert, D., Widdel, F., Gieseke, A., Amann, R., Jørgensen, B.B., Witte, U., Pfannkuche, O., 2000. A marine microbial consortium apparently mediating anaerobic oxidation of methane. Nature 407, 623–626.

Boudreau, B.P., 1997. Diagenetic Models and Their Implementation. Springer Berlin Heidelberg. 414 pp.

Brooks, J.M., Kennicutt, M.C., McDonald, T.J., Fay, R.R., Sassen, R., 1984. Thermogenic gas hydrates in the Gulf of Mexico. Science 225, 409–411.

Brown, K., 1990. The nature and hydrogeologic significance of mud diapirs and diatremes for accretionary systems. J. Geophys. Res. 95, 8969–8982.

Brumsack, H.J., Zuleger, E., 1992. Boron and boroan isotopes in the pore waters from ODP Leg 127, Sea of Japan. Earth Plant. Sci. Lett. 113, 427–433.

Camerlenghi, A., Cita, M.B., Della Vedova, B., Fusi, N., Mirabile, L., Pellis, G., 1995. Geophysical evidence of mud diapirism on the Mediterranean Ridge accretionary complex. Mar. Geophys. Res. 17, 115–141.

Charlou, J.L., Donval, J.P., Zitter, T., Roy, N., Jean-Baptiste, P., Foucher, J.P., Woodside, J., MEDINAUT Scientific Party, 2003. Evidence of methane venting and geochemistry of brines on mud volcanoes of the eastern Mediterranean Sea. Deep-Sea Res. I 50, 941–958.

Colten-Bradley, V.A., 1987. Role of pressure in smectite dehydration—effects on geopressure and smectite–illite transformation. AAPG Bull. 71, 1414–1427.

Dählmann, A., De Lange, G.J., 2003. Fluid–sediment interactions at Eastern Mediterranean mud volcanoes: a stable isotope study from ODP Leg 160. Earth Planet. Sci. Lett. 212, 377–391.

de Lange, G.J., 1992. Shipboard routine and pressure-filtration system for pore water extraction from suboxic sediments. Mar. Geol. 109, 77–81.

de Lange, G.J., Ten Haven, H.L., 1983. Recent sapropel formation in the Eastern Mediterranean. Nature 305, 797–798.

de Lange, G.H., Brumsack, H.-J., 1998. Pore-water indications for the occurrence of gas hydrates in eastern Mediterranean mud dome structures. Proc. ODP Sci. Res. 160, 569–574.

Dia, A.N., Castrec-Rouelle, M., Boulègе, J., Comeau, P., 1999. Trinidad mud volcanoes: where do the expelled fluids come from? Geochim. Cosmochim. Acta 63, 1023–1038.

Egeberg, P.K., Dickens, G.R., 1999. Thermodynamic and pore water halogen constraints on gas hydrate distribution at ODP Site 997 (Blake Ridge). Chem. Geol. 153, 53–79.

Fruehn, J., Reston, T., von Huene, R., Bialas, J., 2002. Structure of the Mediterranean Ridge accretionary complex from seismic velocity information. Mar. Geol. 186, 43–58.

Fusi, N., Kenyon, N.H., 1996. Distribution of mud diapirism and other geological structures from long-range sidescan sonar (GLORIA) data, in the eastern Mediterranean Sea. Mar. Geol. 132, 21–38.

Gieskes, J.M., Blanc, G., Vrolijk, P., Elderfield, H., Barnes, R., 1990. Interstitial water chemistry—major constituents. Proc. ODP Sci. Res. 110, 155–177.

Gieskes, J.M., Gamo, T., Kastner, M., 1993. Major and minor element geochemistry of the interstitial waters of Site 808—Nankai Trough: an overview. Proc. ODP Sci. Res. 131B, 387–396.

Giggenbach, W.F., 1988. Geothermal solute equilibria. Derivation of Na–K–Mg–Ca geoindicators. Geochim. Cosmochim. Acta 52, 2749–2765.

Giggenbach, W.F., 1997. The origin and evolution of fluids in magmatic-hydrothermal systems. In: Barnes, H.L. (Ed.), Geochemistry of Hydrothermal Ore Deposits. John Wiley and Sons, Inc., New York, pp. 737–796.

Ginsburg, G.D., Milkov, A.V., Soloviev, V.A., Egorov, A.V., Cherkashev, G.A., Vogt, P.R., Crane, K., Lorensen, T.D., Khutorskoy, M.D., 1999. Gas hydrate accumulation at the Håkon Mosby mud volcano. Geo Mar. Lett. 19, 57–67.

Haese, R.R., 2002. Macrobenthic activity and its effects on biogeochemical reactions and fluxes. In: Wefer, G., Billet, D., Hebbeln, D., Jørgensen, B.B., Schlüter, M., Van Weering, T. (Eds.), Ocean Margin Systems. Springer-Verlag Berlin Heidelberg, pp. 219–234.

Haese, R.R., Meile, C., Van Cappellen, P., De Lange, G.J., 2003. Carbon geochemistry of cold seeps: methane fluxes and transformation in sediments from Kazan mud volcano, eastern Mediterranean Sea. Earth Planet. Sci. Lett. 212, 361–375.

Han, M.W., Suess, E., 1989. Subduction-induced pore fluid venting and the formation of authigenic carbonates along the Cascadia continental margin: implications for the global Ca-cycle. Paleogeogr. Paleoclim. Paleoecol. 71, 97–118.

Henry, P., Foucher, J.-P., Le Pichon, X., Sibuet, M., Kobayashi, K., Tarits, P., Chamot-Rooke, N., Furuta, T., Schultheiss, P., 1992. Interpretation of temperature measurements from the *Kaiko-Nankai* cruise: Modeling of fluid flow in clam colonies. Earth Planet. Sci. Lett. 109, 355–371.

Henry, P., Le Pichon, X., Lallemant, S., Lance, S., Martin, J.B., Foucher, J.-P., Fiala-Médioni, A., Rostek, F., Guilhaumou, N., Pranal, V., Castrec, M., 1996. Fluid flow in and around mud volcano field seaward of the Barbados accretionary wedge: results from *Manon* cruise. J. Geophys. Res. 101 (B), 20,297–20,323.

Hensen, C., Zabel, M., Pfeifer, K., Schwenk, T., Kasten, S., Riedinger, N., Schulz, H.D., Boetius, A., 2003. Control of sulfate pore water profiles by sedimentary events and the significance of anaerobic oxidation of methane for the burial of sulfur in marine sediments. Geochim. Cosmochim. Acta. 67, 2631–2647.

Hinrichs, K.-U., Hayes, J.M., Sylva, S.P., Brewer, P.G., DeLong, E.F., 1999. Methane-consuming archaebacteria in marine sediments. Nature 398, 802–805.

Hovland, M., Talbot, M.R., Qvale, H., Olaussen, S., Aasberg, L., 1987. Methane-related carbonate cements in pockmarks of the North Sea. J. Sediment. Petrol. 57, 881–892.

Huguen, C., Mascle, J., Chaumillon, E., Woodside, J.M., Benkhelil, J., Kopf, A., Volkonskaïa, A., 2001. Deformation styles of the eastern Mediterranean Ridge and surroundings from combined swath mapping and seismic reflection profiling. Tectonophysics 343, 21–47.

Jongsma, D., Fortuin, A.R., Huson, W., Troelstra, S.R., Klaver, S.T., Peters, J.M., Van Harten, D., De Lange, G.J., Ten Haven, L., 1983. Discovery of an anoxic basin within the Strabo Trench, Eastern Mediterranean. Nature 305, 795–797.

Kastner, M., Elderfield, H., Jenkins, W.J., Gieskes, J.M., Gamo, T., 1993. Geochemical and isotopic evidence for fluid in the western Nankai subduction zone, Japan. Proc. ODP Sci. Res. 131B, 397–416.

Kopf, A., Robertson, A.H.F., Clennell, M.B., Flecker, R., 1998. Mechanisms of mud extrusion on the Mediterranean Ridge accretionary complex. Geo Mar. Lett. 18, 97–114.

Kulm, L.D., Suess, E., Moore, J.C., Carson, B., Lewis, B.T., Titge, rS.D., Kadko, D.C., Thornburg, T.M., Embley, R.W., Rugh, W.D., Massoth, G.J., Langseth, M.G., Cochrane, G.R., Scamman, R.L., 1986. Oregon subduction zone: venting, fauna, and carbonates. Science 231, 561–566.

Land, L.S., Macpherson, G.L., 1992. Origin of saline formation waters, Cenozoic Section, Gulf of Mexico sedimentary basin. AAPG Bull. 76, 1344–1362.

Lemarchand, D., Gaillard, J., Lewin, É., Allègre, C.J., 2000. The influence of rivers on marine boron isotopes and implications for reconstructing past ocean pH. Nature 408, 951–954.

Le Pichon, X., Kobayashi, K., Kaiko-Nankai Scientific Crew, 1992. Fluid venting activity within the eastern Nankai Trough accretionary wedge: A summary of the 1989 Kaiko-Nankai results. Earth Planet. Sci. Lett. 109, 303–318.

Li, Y.-H., Gregory, S., 1974. Diffusion of ions in sea water and in deep-sea sediments. Geochim. Cosmochim. Acta 38, 703–714.

Limonov, A.F., Woodside, J.M., Cita, M.B., Ivanov, M.K., 1996. The Mediterranean Ridge and related mud diapirism: a background. Mar. Geol. 132, 7–19.

Linke, P., Suess, E., Torres, M., Martens, V., Rugh, W.D., Ziebis, W., Kulm, L.D., 1994. In situ measurements of fluid flow from cold seeps at active continental margins. Deep-Sea Res. (I) 41, 721–739.

MacDonald, I.R., Guinasso Jr., N.J., Sassen, R., Brooks, J.M., Lee, L., Scott, K.T., 1994. Gas hydrate that breaches the sea floor on the continental slope of the Gulf of Mexico. Geology 22, 699–702.

Martin, J.B., Kastner, M., Henry, P., Le Pichon, X., Lallement, S., 1996. Chemical and isotopic evidence for sources of fluids in a mud volcano field seaward of the Barbados accretionary wedge. J. Geophy. Res. 101, 20,325–20,345.

Masuzawa, T., Handa, N., Kitagawa, H., Kusakabe, M., 1992. Sulfate reduction using methane in sediments beneath a bathyal cold seep giant clam community off Hatsushima Island, Sagami Bay, Japan. Earth Planet. Sci. Lett. 110, 39–50.

MEDINAUT/MEDINETH Shipboard Scientific Parties, 2000. Linking Mediterranean brine pools and mud volcanism. EOS 81 625, 631–632.

Moore, J.C., Vrolijk, P., 1992. Fluids in accretionary prisms. Rev. Geophys. 30, 113–135.

Morton, R.A., Land, L.S., 1987. Regional variations in formation water chemistry, Frio Formation (Oligocene), Texas Gulf Coast. AAPG Bull. 71, 191–206.

Olu-Le Roy, K., Sibuet, M., Fiala-Médioni, A., Gofas, S., Salas, C., Mariotti, A., Foucher, F.-P., Woodside, J., 2004. Cold seep communities in the deep eastern Mediterranean Sea: composition, symbiosis and spatial distribution on mud volcanoes. Deep Sea Res. 51, 1915–1936.

Pancost, R.D., Sinninghe Damsté, J.S., De Lint, S., Van Der Maarel, M.J.E.C., Gottschal, J.C., The MEDINAUT Shipboard Scientific Party, 2000. Biomarker evidence for widespread anaerobic methane oxidation in Mediterranean sediments by a consortium of methanogenic archaea and bacteria. Appl. Environ. Microbiol. 66, 1126–1132.

Pfeifer, K., Hensen, C., Adler, M., Wenzhöfer, F., Weber, B., Schulz, H.D., 2002. Modeling of subsurface calcite dissolution regarding respiration and reoxidation processes in the equatorial upwelling off Gabon. Geochim. Cosmochim. Acta 66, 4247–4259.

Savenko, A.V., Tsytsarin, A.G., Povalishnikova, E.S., 2002. Behavior of strontium, fluorine, and boron in Kuban and Don mouth areas. Water Res. 29, 676–685.

Schulz, H.-M., Emeis, K.-C., Volkman, N., 1997. Organic carbon provenance and maturity in the mud breccia from the Napoli mud volcano: indicators of origin and burial depth. Earth Planet. Sci. Lett. 147, 141–151.

Sibuet, M., Olu, K., 1998. Biogeography, biodiversity and fluid dependence of deep-sea cold seep communities at active and passive margins. Deep Sea Res. (II) 45, 517–567.

Stoll, M., Bakker, K., Nobbe, G.H., Haese, R.R., 2001. Continuous flow analysis of dissolved inorganic carbon content in sea water. Anal. Chem. 73, 4111–4116.

Suess, E., Bohrmann, G., von Huene, R., Linke, P., Wallmann, K., Lammers, S., Sahling, H., 1998. Fluid venting in the eastern Aleutian subduction zone. J. Geophys. Res. 103, 2597–2614.

Suess, E., Torres, M.E., Bohrmann, G., Collier, R.W., Greinert, J., Linke, P., Rehder, G., Trehu, A., Wallmann, K., Winckler, G., Zuleger, E., 1999. Gas hydrate destabilization: enhanced dewatering, benthic material turnover and large methane plumes at the Cascadia convergent margin. Earth Planet. Sci. Lett. 170, 1–15.

Ten Veen, J.H., Woodside, J.M., Zitter, T.A.C., Dumont, J.F., Mascle, J., Volkonskaïa, A., 2004. Neotectonic evolution of the Anaximander Mountains at the junction of the Hellenic and Cyprus arcs. Tectonophysics 391, 35–65.

Vengosh, A., De Lange, G.J., Starinsky, A., 1998. Boron isotope and geochemical evidence for the origin of Urania and Bannock brines at the eastern Mediterranean: effect of water–rock interactions. Geochim. Cosmochim. Acta 62, 3221–3228.

Von Huene, R., Scholl, D.W., 1991. Observations at convergent margins concerning subduction, subduction erosion, and the growth of continental crust. Rev. Geophys. 29, 279–317.

Vrolijk, P., 1990. On the mechanical role of smectite in subduction zones. Geology 18, 703–707.

Wallmann, K., Linke, P., Suess, E., Bohrmann, G., Sahling, H., Schlüter, M., Dählmann, A., Lammers, S., Greinert, J., von Mirbach, N., 1997. Quantifying fluid flow, solute mixing, and biogeochemical turnover at cold vents of the eastern Aleutian subduction zone. Geochim. Cosmochim. Acta 61, 5209–5219.

Westbrook, G.K., Reston, T.J., 2002. The accretionary complex of the Mediterranean Ridge: tectonics, fluid flow and the formation of brine lakes. Mar. Geology 186, 1–8.

Whiticar, M.J., 1999. Carbon and hydrogen isotope systematics of bacterial formation and oxidation of methane. Chem. Geol. 161, 291–314.

Wilson, T.R.S., Thomson, J., Hydes, D.J., Colley, S., Culkin, F., Sørensen, J., 1986. Oxidation fronts in pelagic sediments: diagenetic formation of metal-rich layers. Science 323, 972–975.

Woodside, J.M., Ivanov, M.K., Limonov, A.F., Shipboard Scientists of the Anaxiprobe Expeditions, 1998. Shallow gas and gas hydrates in the Anaximander Mountains regions, eastern Mediterranean Sea. In: Henriet, J.-P., Minert, J. (Eds.), Gas Hydrates: Relevance to World Margin Stability and Climate Change, Geological Society. Spec. Publ., vol. 137, pp. 177–193. London.

You, C.-F., Spivack, A.J., Smith, J.H., Gieskes, J.M., 1993. Mobilization of boron in convergent margins: implications for the boron geochemical cycle. Geology 21, 207–210.

You, C.-F., Spivack, A.J., Gieskes, J.M., Martin, J.B., Davisson, M.L., 1996. Boron contents and isotopic compositions in pore waters: a new approach to determine temperature induced artifacts—geochemical implications. Mar. Geol. 129, 351–361.

Zuleger, E., Gieskes, J.M., You, C.-F., 1996. Interstitial water chemistry of sediments of the Costa Rica accretionary complex off the Nicoya Peninsula. Geophys. Res. Lett. 23, 899–902.